A Low Cost and Compact RF Switching System for Wearable Microwave Head Imaging with Performance Verification on Artificial Head Phantom

IET Microwaves, Antennas & Propagation

A Low Cost and Compact RF Switching System for Wearable Microwave Head Imaging with Performance Verification on Artificial Head Phantom

Mohd Saiful Riza Bashri, Tughrul Arslan

School of Engineering, University of Edinburgh, Edinburgh, United Kingdom
*m.bashri@ed.ac.uk.com

Abstract: This paper presents a low cost, compact and lightweight RF switching system for wearable head imaging applications. The proposed switching system is made from commercial off-the-shelf components (COTS). The switching system provides a wideband performance which covers operating frequency band from DC to 4 GHz. A low power microcontroller is integrated with two RF switches as a control system. An array of twelve wideband monopole antennas were connected to the proposed switching circuit and its performance was evaluated using an artificial human head phantom. To verify the performance of the system, a haemorrhagic stroke was mimicked by placing a spherical target of 30 mm in diameter inside the fabricated head phantom. Two data acquisition methods were applied using the switching system. In the first method, the reflection coefficients of the antennas were collected for healthy and unhealthy brain injury cases. For the second method, the transmission coefficients of the antennas were collected by utilising four antennas in the array as transmitting antennas while the rest of the antennas act as receiving antennas. We demonstrates that the proposed compact switching system could be used for future real-time wearable detection systems embedded in various headgear products.

1. Introduction

Over the past few decades, microwave imaging for medical applications has attracted significant interest due to its many advantages such as low cost, fast, non-invasive and non-ionisation characteristics [1]. Microwave imaging techniques provide an alternative method to conventional modalities such as computed tomography, magnetic resonant imaging system, and ultrasound for detection of various diseases inside a human body. One of the widely research area in medial microwave imaging is radar-based systems which utilise ultra-wideband antennas to create a useful image of diseases inside a human body. Several attempts on using radar-based microwave systems have been reported for early detection of breast cancer [2–4]. A clinical trial was conducted on real patients for breast cancer detection shows the feasibility of using microwave technology to complement the existing medical imaging systems in the future [5].

Recently, microwave technology has also been utilised for head imaging and detection of diseases such as stroke and traumatic brain injury [6–8]. Compared to breast, human head has more complex biological structure which consists of several lossy tissue layers and skull [9]. Feasibility study of using ultra-wideband (UWB) microwave technology for head imaging technique has been carried out using simulation tools as presented in [10]. It is reported that that there is detectable difference between the scattered signals from a healthy head and a head embedded with tumour. The proposed Vivaldi antenna used high operating frequency range thus limits the penetration depth of the electromagnetic wave inside the head model and only tumour close to the outer head region could be detected. Moreover, no switching system was used since the antenna was manually positioned around the head.

A microwave head imaging systems utilising UWB Vivaldi antennas for stroke detection was presented in [11]. An array of 16 Vivaldi antennas was positioned around the artificial head phantom where the distance between the antennas and the head phantom was kept at 0.5 cm. An ellipsoidal-shaped target of size 2 cm × 1 cm × 0.5 cm was inserted into the head phantom to mimic the occurrence of haemorrhagic stroke. The proposed system was successful in showing the location of the stroke target. The switching system implemented in this work utilised microwave coaxial switches in order to connect the elements of the array. The size of the switching device is relatively large and only suitable for a static testing environment.

A portable microwave head imaging system to detect traumatic brain injuries was reported in [6] by utilising a compact directional antenna and microwave transceiver. The proposed system was tested on a realistic human head phantom to verify its detection capabilities. The antenna was rotated at 32 different angular positions to scan the head phantom. Since there was only one antenna used in the setup, no switching device is required.

The microwave head imaging systems above were developed to operate either in static diagnostic setup at hospitals or as a portable system such as in an ambulance to provide rapid response to patients. Recently, there have been an emerging trend of using wearable devices to monitor a person health in real-time [12]. The wearable devices could be embedded or integrated inside a person's garment to act as a sensing or imaging system [13]. By providing a real-time detection, an alerting system could be set up where rapid

response could be delivered. In addition, a medical database could be created to store the measured signals which could be used for future analysis which would help identifying fatal diseases in advance. The wearable health detection concept could potentially prevent a patient from suffering a permanent health damage or in extreme cases from dying such as a person suffering from stroke. An example of the wearable system for health monitoring is a wearable pulmonary edema monitoring sensor presented in [14]. The sensor is made of 17 electrodes with 16 ports in-between where it will be placed on the human chest. The system was built to detect lung irregularities by measuring the lung's average permittivity in a non-invasive way. The system was integrated with body-area network (BAN) to provide remote data transfer. On the other hand, a wearable system for breast cancer detection is presented in [15]. 4 × 4 antenna array was developed in a bra-like format. The antenna design was validated on a phantom mimicking breast tissue. However, no switching system is proposed in this work. A flexible circuit board integrated with solid-state switching network and 16 wideband antennas is presented in [16]. By integrating the switching matrix and the antenna array on the same substrate, the overall size of the microwave imaging system was reduced. The idea of using compact RF switch system paves the way for future wearable microwave medical imaging applications.

In order to move towards wearable systems for head sensing or imaging, it is first necessary to replace some of the main components in the system with smaller and eventually wearable solutions. As a proof of concept, a compact and lightweight RF switching system is presented in this paper using commercial off-the-shelf components. This study is a modified version of our work presented in [17], with the major improvement of using an additional solid-state switch which is one-pole four-throw (1P4T) type in combination with the previous one-pole eight-throw (1P8T) switch. The utilisation of two RF solid-state switches in the switching system permits the use of two data acquisition methods namely reflection coefficient and transmission coefficient as compared to only the former method in the previous work. In the first method, the two switches are combined to form a single-pole twelve throw (1P12T) switch which can accommodate an additional four antennas in the wearable imaging system. In this case, 12 antennas could be utilised in the system. For the next method, a total of 32 transmission coefficient channels could be measured. This is realised by using the 1P4T switch for the transmitting antennas and the 1P8T switch for the receiving antennas. To investigate the performance of the switches, measurements were carried out separately for each of the switches in terms of their impedance matching and insertion loss.

To further verify the feasibility of the proposed switching system, the switching circuit is connected to an array of twelve wideband flexible monopole antennas previously presented in [18] for evaluation using a realistic head phantom. Measurement results for the final design of the proposed system are discussed and analysed. It is intended that the proposed compact and low cost RF switching system to serve as a proof of concept for future development of real-time monitoring wearable head imaging systems.

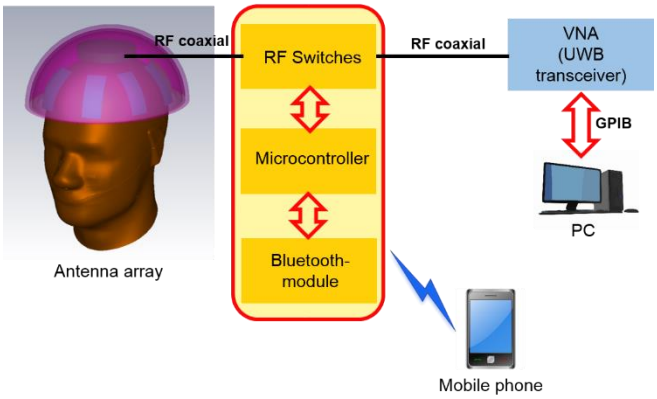

Fig. 1. *Diagram of the proposed RF switching system*

2. RF Switching System Architecture

To realise a wearable head imaging system, a compact and lightweight RF switching circuit for an antenna array (sensors) is developed using commercial off-the-shelf (COTS) components. Two evaluation boards of MMIC single-pole eight-throw (1P8T) switch, HMC321LP4E and single-pole four-throw (1P4T) switch, HMC241ALP3E from Analog Device are chosen [19][20]. The switches offer wideband operating frequency range from DC to 4 GHz which is sufficient to cover the operating frequency typically used for head imaging application. In order to provide enough penetration and sensible resolution inside the human head, most of the research in the literature utilise frequency band between 1GHz to 4GHz [6, 11, 21]. The diagram of the proposed switching architecture is shown in Fig. 1.

In order to operate the switches, an Arduino Nano board from Arduino was chosen based on several criteria mainly its compact size and low power consumption. Both of the switches and the board operate at 5 V and could be easily powered up using a 9 V battery. The microcontroller embedded inside the Arduino Nano, Atmel ATMega328, consumes only 0.2 mA during its operation mode. The reason for integrating a microcontroller with the switches is due to further prove the wearable concept for head imaging system where it would be integrated with ultra-wideband transceiver as system on a chip (SoC) in the future work. However, in this research, the main function of the micro-controller is to control the switches during operation and testing.

Five control pins from the Arduino board are connected to both of the switches which will control the selection of each individual port. A wireless connection is also implemented on the system to control the proposed switching circuit using an android based smartphone via Bluetooth module. The selection of Bluetooth module was due to its low power usage compared to WiFi module thus further reducing the power consumption of the overall system. An android application was coded and installed into a mobile phone to provide the graphical user interface.

To investigate the performance of the RF switches, their insertion losses (S_{21}) at frequency band up to 3 GHz were measured using a vector network analyser at all the ports as illustrated in Fig. 2. Next, their impedance matching performance was evaluated in terms of reflection coefficient. Finally, the proposed switching system was then connected to an array of twelve ultra-wideband monopole antennas. The reflection and transmission coefficient measurements were taken with the presence of an artificial head phantom for further analysis.

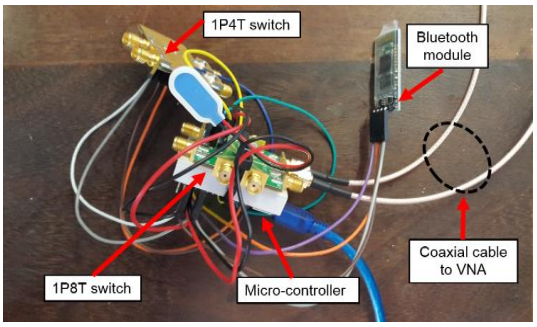

(a)

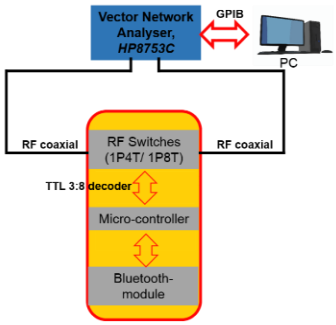

(b)

Fig. 2. *(a) Photograph and (b) the diagram of the measurement setup for the RF switches*

3. Measurements of the solid-state RF switches

The performance of both of the switches is first evaluated in terms of their insertion losses and reflection coefficients at each of the RF port. The measurements were carried out using the two-port vector network analyser, HP8753C. Due to the limitation of the VNA, only measurements up to 3 GHz could be conducted. Nevertheless, considering that the RF switches are to be used for microwave head imaging and detection systems, most of the antennas designed for these applications work below 3 GHz in order to provide enough electromagnetic wave penetration inside the human head [6][22]. The insertion losses of the 1P4T switch and the 1P8T switch are shown in Fig. 3 and Fig. 4 respectively. It can be seen that the insertion loss of the 1P4T switch is lower than the 1P8T switch by 1.06 dB up to 3 GHz. The maximum measured insertion loss at 2.5 GHz is -2.54 dB at port 7 of the

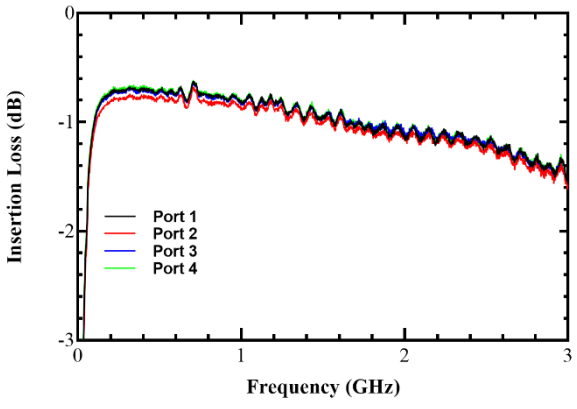

Fig. 3. *Measured insertion loss of single-pole-four-throw (1P4T) RF switch*

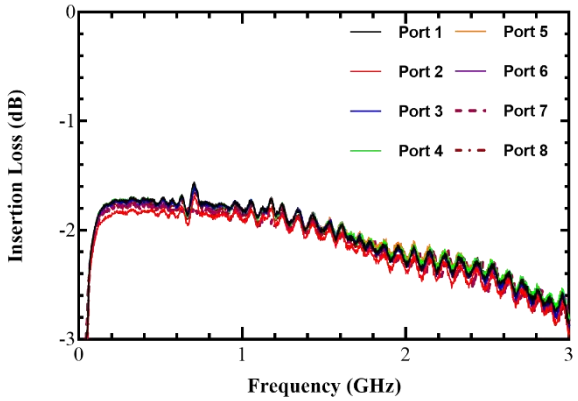

Fig. 4. *Measured insertion loss of single-pole-eight-throw (1P8T) RF switch*

1P8T switch.

The switches' reflection coefficient characteristics are illustrated in Fig. 5 and Fig. 6 respectively. The average measured reflection coefficients of the 1P4T and 1P8T switches at 2.5 GHz are -26.2 dB and -18.9 dB. The maximum measured reflection coefficient value is -17.5 dB at port 7 of the 1P8T switch. The difference in S_{11} responses between the two switches is mainly due to the manufacturing factor. Nevertheless, the measurement results show excellent impedance matching characteristic up to 3 GHz which match the values provided by the datasheets. It is important to ensure that the switches' impedance matching performance would not deteriorate the performance of the antenna array that is to be integrated later in the final system.

To further validate the performance of the switching system, an array of twelve wideband monopole antennas is connected to the switches. An artificial head phantom that mimics the electrical properties of the actual human head was fabricated as shown in Fig. 7. The soft brain tissue was created by mixing tab water, sugar, agar and salt following the procedures proposed in [7]. However, the proportions of the materials was slightly changed due to the use of tab water instead of deionised water in order to get similar electrical properties of actual grey matter [23]. The recipes of the head phantom is provided in Table I. In addition, a liquid mimicking blood will be used to mimic the occurrence of haemorrhagic stroke inside the head phantom.

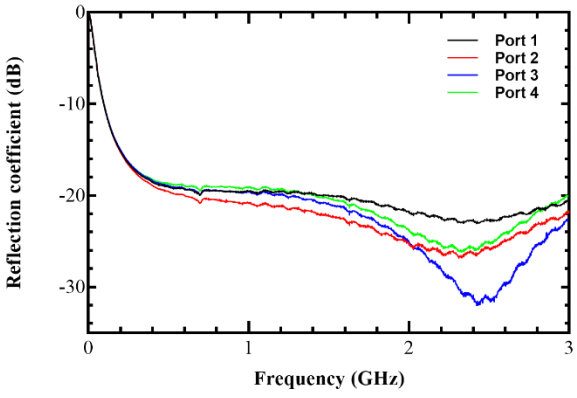

Fig. 5. *Measured reflection coefficient of the single-pole-four-throw (1P4T) RF switch*

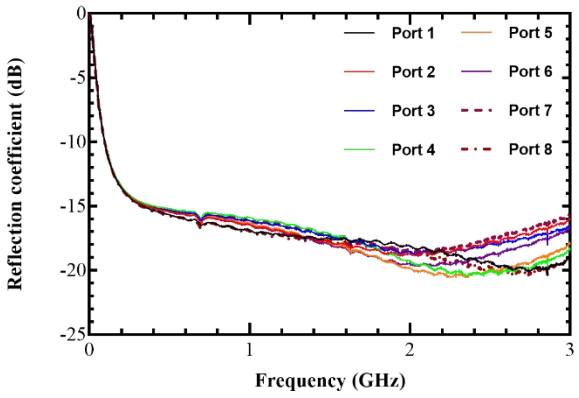

Fig. 6. *Measured reflection coefficient of the single-pole-eight-throw (1P8T) RF switch*

4. Performance Verification using an Artificial Head Phantom

Most of the wideband microwave techniques for head imaging or detection applications rely on the differences of the reflection coefficients and/or transmission coefficients between a healthy brain and unhealthy brain i.e. stroke induced condition or traumatic brain injuries [7, 11, 22, 24]. The blood clot inside the brain causes the reflection coefficient of the transmitting antennas to change depending on its distance from the antenna and size. On the other hand, it has been reported in [7] that the transmission coefficients of the antenna pair where a blood clot was positioned along its path show noticeable differences between healthy and various clot sizes. By exploiting these findings, two methods of data acquisition could be applied for wearable imaging systems using the proposed RF switching system. In this section, we will investigate and compare both of the methods by mimicking injuries inside the brain by placing a spherical target that mimics the formation of a blood clot inside the head. Moreover, to verify the performance of the proposed switching system, an imaging algorithm based on confocal delay-and-sum (CDAS) algorithm is utilised to determine the location of the stroke inside the head phantom [11, 25, 26].

Fig. 7. *Fabricated artificial head phantom*

Table 1 Recipes for grey matter and blood

Ingredients	Grey matter (%)	Blood (%)
Tab water	50	70
Sugar	50	30
Agar	15	-
Salt	0.1	0.2
Sodium Benzoate	0.1	-

4.1. Reflection coefficient (S_{11}) measurements

For our initial investigation, we use differential signals where a head scan with a healthy head (no bleeding) and then with a head phantom with a blood clot. The size of the spherical blood clot placed inside the head phantom is 30 mm in diameter as shown in Fig.8. The reflection coefficients of the antennas closer to the blood clot are then compared between these two scenarios. Since there are twelve antennas in the array, twelve reflection coefficient responses were recorded as shown in Fig. 9 and Fig. 10 for healthy and unhealthy cases respectively. This method can be viewed as mono-static radar approach where only one antenna is active at a certain time. The location of the antennas placed on the head phantom is shown in Fig. 11 where the lossy dielectric absorber was removed for clarity. During the measurements, the absorber was attached to the antennas to suppress the back lobe radiation in order to prevent the system from measuring the unwanted surrounding noise. Based on Fig. 12, it can be seen that the reflection coefficient values of the three antennas (referred as Ant1, Ant2 and Ant3) which locations were the closest to the spherical target show noticeable differences between healthy and unhealthy head which confirms the finding reported in [27] . This is due to the changes in the dielectric constant of the materials along the propagation path of the signal transmitted and received by those antennas due to the existence of the blood clot. As for the other antennas, their responses were not affected since the blood clot was not within their signal propagation paths or their location were too far from the target. By using this information, an image of the location of the blood clot is

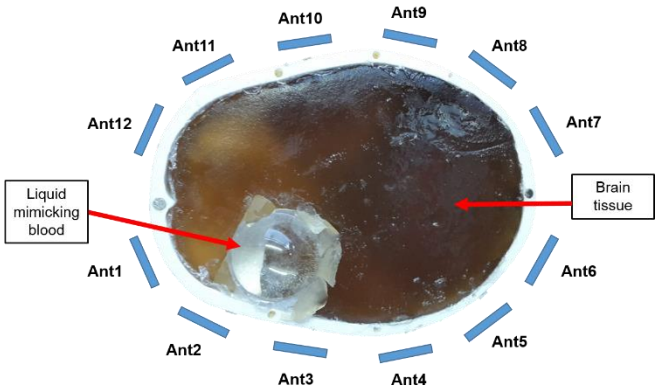

Fig. 8. *Location of the blood clot inside the head phantom*

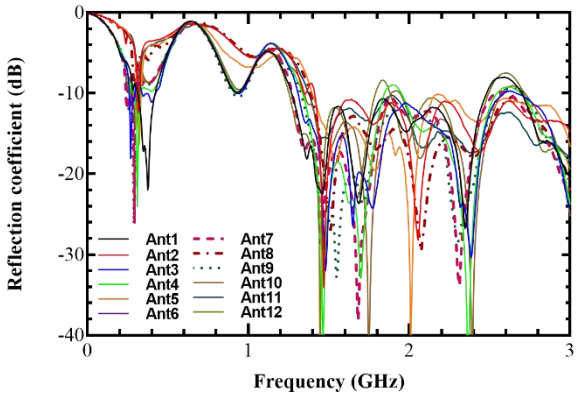

Fig. 9. *Measured reflection coefficient of the antennas with the presence of healthy head phantom*

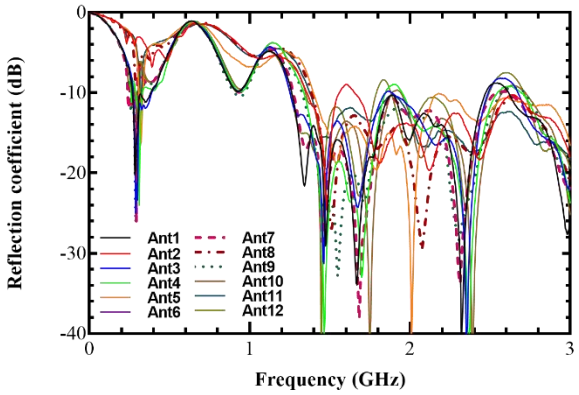

Fig. 10. *Measured reflection coefficient of the antennas with the presence of unhealthy head phantom*

created by applying the CDAS algorithm [6, 11]. Since the data is collected in the frequency domain, an inverse discrete fast Fourier transform (IDFT) is applied to the reflection coefficients to convert it to the time domain signal. The differential signals are input into the imaging algorithm to remove any unwanted reflections from the surrounding [15]. The images of the head for healthy and unhealthy cases are shown in Fig. 13. As a comparison with a system without the RF switching circuit, another image of the head with the stroke created without utilising the switching circuit is also shown. Both images show that the stroke is clearly detected and localised. This indicates that the proposed RF switching circuit gives similar performance compared to the system without the switching circuit. The resolution and accuracy of the imaging system can be improved by using more antennas at the expense of larger wearable device to accommodate the additional antennas and increased data acquisition time.

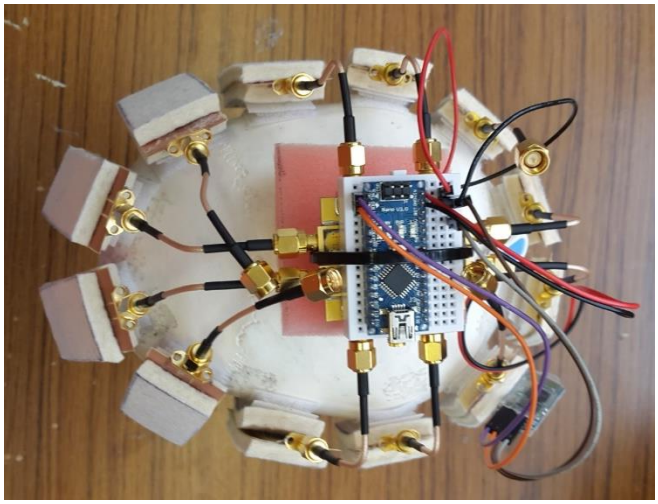

Fig. 11. *Location of the antennas and the switching system (top view)*

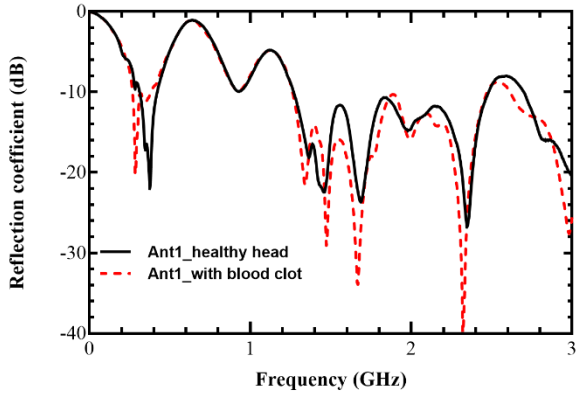

(a)

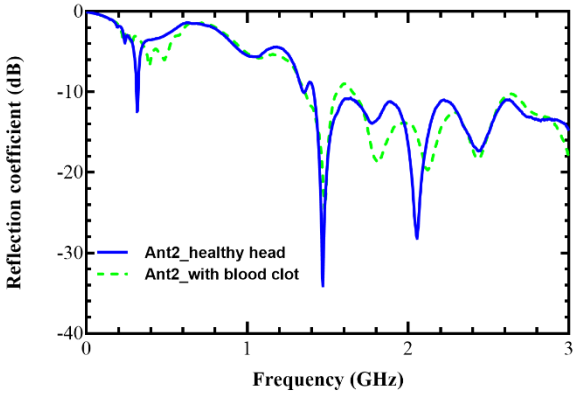

(b)

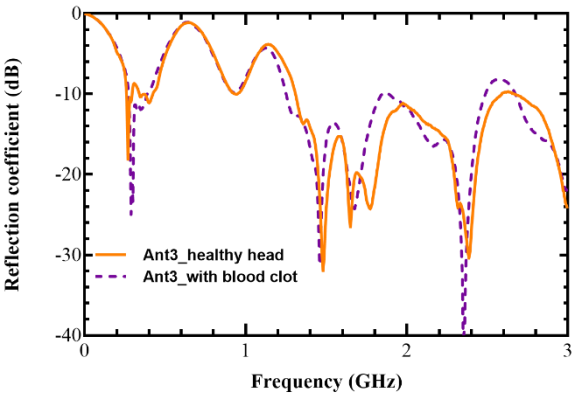

(c)

Fig. 12. *Measured reflection coefficient of the antennas with healthy and unhealthy head*
(a) *Ant1* ***(b)*** *Ant2* ***(c)*** *Ant3*

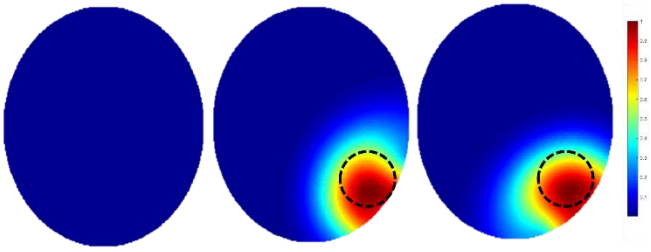

(a) *(b)* *(c)*

Fig. 13. *Imaging results for (a) healthy head and unhealthy head (b) without the switching circuit (c) and with the switching circuit. The exact locations of the bloods are indicated by the dashed black circles.*

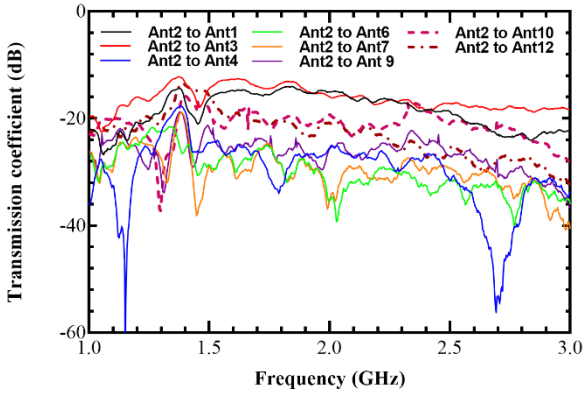

Fig. 14. *Measured transmission coefficients between antenna 2 and the receiving antennas for healthy head phantom*

4.2. Transmission coefficient measurements

By using four of the antennas from the array as transmitting antennas and the remaining eight antennas as receiving antennas, thirty two transmission coefficient channels were collected for both scenarios. This method has been implemented in [7, 8] for the detection of subdural hematoma and stroke types where machine learning algorithms are utilised for the classification of the diseases. In this method, the 1P4T switch is connected to the four transmitting antennas while the remaining eight antennas are connected to the 1P8T switch. The amplitudes of S_{21} were measured for all the thirty two communication channel pairs.

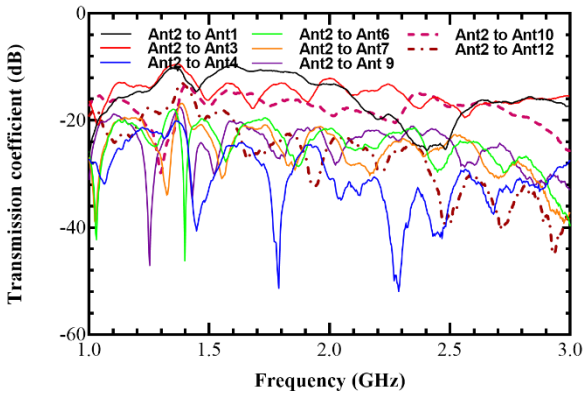

Fig. 15. *Measured transmission coefficients between antenna 2 and the receiving antennas for unhealthy head phantom*

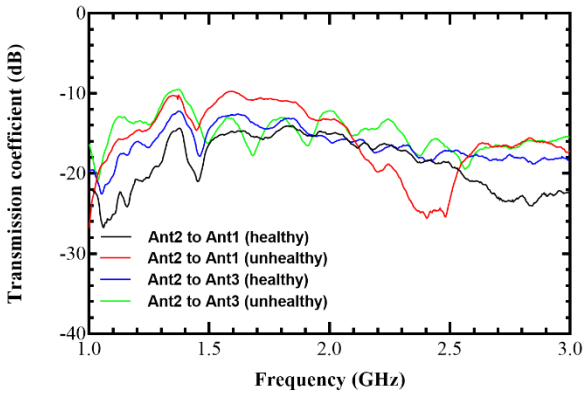

Fig. 16. *Measured transmission coefficients of the antennas with healthy and unhealthy head for antenna 2-antenna 1and antenna 2-antenna 3*

However, for brevity only S_{21} between antenna 2 (as transmitting antenna) and the eight receiving antennas will be analysed. The measured S_{21} results between antenna 2 and the receiving antennas are plotted in Fig. 14 and Fig. 15 for both healthy and unhealthy head conditions. In general, from the S_{21} results, we can conclude that antenna pairs that are further apart have higher insertion loss due to longer path taken by the signal to travel between them. Moreover, the insertion loss also increases with frequency since the head phantom and biological tissues in general have higher loss at higher frequencies. To investigate the differences in amplitude of S_{21} between healthy and unhealthy cases, the transmission coefficients for two antenna pairs namely Ant2-Ant1 and Ant2-Ant3 are plotted in Fig. 16. It can be seen that the insertion loss for antenna 2 and antenna 1 pair for the unhealthy case is lower than the healthy case between 2 GHz to 2.5 GHz. This could be attributed to the existence of the blood clot in the path of the antenna pair where the higher conductivity of the blood clot compared to the brain tissue causes the transmission path loss to increase. The trend could also be observed for Ant2-Ant3 pair at 1.6 GHz and 2.5 GHz frequency range where the transmission loss is higher for the unhealthy case than the heathy brain due to the formation of the blood clot in its path. Nevertheless, by applying advanced post-processing techniques such as machine learning algorithm, detection or imaging of potential head diseases such as stroke or traumatic brain injuries could be implemented using this transmission coefficient method.

5. Conclusion

In this work, a low cost, compact and lightweight RF switching system for wearable microwave head imaging has been presented. Two monolithic microwave integrated circuit (MMIC) RF switches which consist a single-pole-four-throw (1P4T) switch and a single-pole-eight-throw (1P8T) switch are utilised in the system. The switching system offers wideband characteristic covering frequency band from DC to 4 GHz. A low power microcontroller is integrated with the switches to control the switches via Bluetooth connection. The maximum measured insertion loss and reflection coefficient are -2.54 dB and -18.9 dB respectively. An array of twelve wideband flexible antennas was connected to the switching system and tested on an artificial human head phantom. Experiment results show that there were noticeable

difference in both reflection coefficients and transmission coefficients when the antenna array was used to scan between a healthy head phantom and a head phantom with a blood clot of size 30 mm in diameter. The location of the blood clot was successfully detected by applying the confocal delay-and-sum imaging technique. The proposed switching system serves as a proof of concept for future development of real-time monitoring wearable head imaging systems.

6. References

1 Fear, E.C., Meaney, P.M., Stuchly, M.A.: 'Microwaves for breast cancer detection?'*Potentials, IEEE*, 2003, **22**, pp. 12–18.

2 Fear, E.C., Stuchly, M.A.: 'Microwave detection of breast cancer'*IEEE Trans. Microw. Theory Tech.*, 2000, **48**, (11), pp. 1854–1863.

3 Porter, E., Bahrami, H., Santorelli, A., Gosselin, B., Rusch, L.A., Popovic, M.: 'A wearable microwave antenna array for time-domain breast tumor screening'*IEEE Trans. Med. Imaging*, 2016, **35**, (6), pp. 1501–1509.

4 Bond, E.J., Li, X., Hagness, S.C., Van Veen, B.D.: 'Microwave imaging via space-time beamforming for early detection of breast cancer'*IEEE Trans. Antennas Propag.*, 2003, **51**, (8), pp. 1690–1705.

5 Preece, A.W., Craddock, I., Shere, M., Jones, L., Winton, H.L.: 'MARIA M4: clinical evaluation of a prototype ultrawideband radar scanner for breast cancer detection'*J. Med. Imaging*, 2016, **3**, (3), p. 33502.

6 Mobashsher, A.T., Abbosh, A.M., Wang, Y.: 'Microwave system to detect traumatic brain injuries using compact unidirectional antenna and wideband transceiver with verification on realistic head phantom'*IEEE Trans. Microw. Theory Tech.*, 2014, **62**, (9), pp. 1826–1836.

7 Candefjord, S., Winges, J., Malik, A.A., *et al.*: 'Microwave technology for detecting traumatic intracranial bleedings: tests on phantom of subdural hematoma and numerical simulations'*Med. Biol. Eng. Comput.*, 2016, pp. 1–12.

8 Persson, M., Fhager, A., Dobsicek Trefna, H., *et al.*: 'Microwave-based stroke diagnosis making global prehospital thrombolytic treatment possible'*IEEE Trans. Biomed. Eng.*, 2014, **61**, (11), pp. 2806–2817.

9 Ireland, D., Bialkowski, M.E.: 'Microwave head imaging for stroke detection'*Prog. Electromagn. Res. M*, 2011, **21**, pp. 163–175.

10 Zhang, H., Flynn, B., Erdogan, A.T., Arslan, T.: 'Microwave imaging for brain tumour detection using an UWB Vivaldi Antenna array'*Loughbrgh. Antennas Propag. Conf.*, 2012, (November).

11 Mohammed, B.J., Abbosh, A.M., Mustafa, S., Ireland, D.: 'Microwave system for head imaging'*IEEE Trans. Instrum. Meas.*, 2014, **63**, (1), pp. 117–123.

12 Zheng, Y.L., Ding, X.R., Poon, C.C.Y., *et al.*: 'Unobtrusive sensing and wearable devices for health informatics'*IEEE Trans. Biomed. Eng.*, 2014, **61**, (5), pp. 1538–1554.

13 Kiourti, A., Volakis, J.L.: 'Wearable antennas using electronic textiles for RF communications and medical monitoring'*2016 10th Eur. Conf. Antennas Propagation, EuCAP 2016*, 2016.

14 Salman, S., Wang, Z., Colebeck, E., Kiourti, A., Topsakal, E., Volakis, J.L.: 'Pulmonary edema monitoring sensor with integrated body-area network for remote medical sensing'*IEEE Trans. Antennas Propag.*, 2014, **62**, (5), pp. 2787–2794.

15 Bahramiabarghouei, H., Porter, E., Gosselin, B., Popovi, M., Rusch, L.A.: 'Flexible 16 antenna array for microwave breast cancer detection'*IEEE Trans. Biomed. Eng.*, 2015, **62**, (10), pp. 2516–2525.

16 Santorelli, A., Porter, E., Kang, E., Piske, T., Popovi, M., Schwartz, J.D.: 'A Time-Domain Microwave System for Breast Cancer Detection Using a Flexible Circuit Board'*IEEE Trans. Instrum. Meas.*, 2015, **64**, (11), pp. 2986–2994.

17 Bashri, M.S.R., Arslan, T., Zhou, W., Haridas, N.: 'A compact RF switching system for wearable microwave imaging', in 'Loughborough Antennas & Propagation Conference (LAPC)' (2016), pp. 2–5

18 Bashri, M.S.R., Arslan, T., Zhou, W., Haridas, N.: 'Wearable device for microwave head imaging', in '46th European Microwave Conference (EuMC)' (2016), pp. 671–674

19 'GaAs MMIC SP8T Non-reflective positive control switch', http://www.analog.com/media/en/technical-documentation/data-sheets/hmc321.pdf

20 'GaAs MMIC SP4T non-reflective positive control switch', http://www.analog.com/media/en/technical-documentation/data-sheets/hmc241alp3e.pdf

21 Ahdi Rezaeieh, S., Zamani, A., Abbosh, A.M.: 'Three Dimensional Wideband Antenna for Head Imaging System with Performance Verification in Brain Tumor Detection'*IEEE Antennas Wirel. Propag. Lett.*, 2015, **14**, pp. 910–914.

22 Mobashsher, A.T.: 'Wideband Microwave Imaging System for Brain Injury Diagnosis'. 2016

23 Gabriel, S., Lau, R.W., Gabriel, C.: 'The dielectric properties of biological tissues:II. Measurements in the frequency range 10Hz to 20 GHz'*Phys Med Biol*, 1996, **41**, (11), pp. 2251–2269.

24 Mohammed, B.J., Abbosh, A.M., Ireland, D.: 'Stroke Detection Based on Variations in Reflection Coefficients of Wideband Antennas', in 'IEEE Antennas and Propagation Society International Symposium (APSURSI)' (2012), pp. 1–2

25 Li, X., Hagness, S.C.: 'A confocal microwave imaging algorithm for breast cancer detection'*IEEE Microw. Wirel. Components Lett.*, 2001, **11**, (3), pp. 130–132.

26 Fear, E.C., Sill, J., Stuchly, M.A.: 'Experimental feasibility study of confocal microwave imaging for breast tumor detection'*IEEE Trans. Microw. Theory Tech.*, 2003, **51**, (3), pp. 887–892.

27 Mobashsher, A.T., Abbosh, A.M.: 'Compact 3-D Slot-Loaded Folded Dipole Antenna with Unidirectional Radiation and Low Impulse Distortion for Head Imaging Applications'*IEEE Trans. Antennas Propag.*, 2016, **64**, (7), pp. 3245–3250.